Q Control of an Atomic Force Microscope Microcantilever: A Sensorless Approach

Matthew W. Fairbairn, *Student Member, IEEE*, S. O. Reza Moheimani, *Fellow, IEEE*, and Andrew J. Fleming, *Member, IEEE*

***Abstract*—The scan rate and image resolution of the atomic force microscope (AFM) operating in tapping-mode may be improved by modifying the quality (Q) factor of the AFM microcantilever according to the sample type and imaging environment. Piezoelectric shunt control is a new method of controlling the Q factor of a piezoelectric self-actuating AFM microcantilever. The mechanical damping of the microcantilever is controlled by an electrical impedance placed in series with the tip oscillation circuit. A synthetic impedance was designed to allow easy modification of the control parameters which may vary with environmental conditions. The proposed techniques are experimentally demonstrated to reduce the Q factor of an AFM microcantilever from 297.6 to 35.5. AFM images obtained using this method show significant improvement in both scan rate and image quality. [2011-0123]**

***Index Terms*—Atomic force microscope (AFM), AFM probe, microcantilevers, microsensors, piezoelectric cantilever, piezoelectric shunt control, synthetic impedance, tapping-mode AFM.**

I. Introduction

THE ATOMIC force microscope (AFM) [1] senses interatomic forces occurring between a sharp probe tip and a sample surface to produce images of sample surfaces such as ceramic materials, biological membranes, metals, polymers, and semiconductors with subnanometer resolution [2]–[6]. The images produced are 3-D with resolution on the order of 0.1 to 1 nm.

The AFM uses a microcantilever, with a sharp probe tip on its lower surface, which is scanned over a sample surface. Deflection of the cantilever, due to interatomic forces between the probe tip and the sample, at each scan point is representative of the sample height. By plotting the sample height versus the horizontal position of the probe, a 3-D image of the surface can be obtained.

The high image resolution of the AFM is due to the size of the probe tip, which may be only a few atoms wide. This gives the AFM an advantage over optical microscopes, which are limited by the wavelength of visible light, which is approximately 400–700 nm.

One of the main advantages of the AFM over other types of nonoptical microscopy is that it can image samples under natural conditions (e.g., in air or liquid). There is no need to place the sample in vacuum, coat it with metal, or dry it, which may cause damage to a living sample, making the AFM particularly useful for biological investigations [7], [8]. One drawback of the AFM compared to an optical microscope is that it takes some time to obtain an image, whereas the optical microscope can produce images in real time.

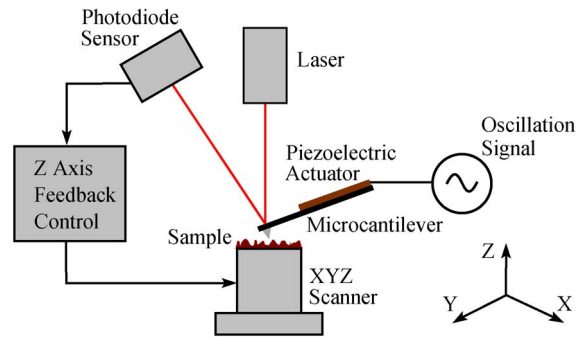

Fig. 1. Schematic of the instrumentation of an AFM operating in tapping mode.

Most commonly, the probe tip is dragged across the sample in constant contact, which is referred to as contact-mode imaging. Continuous lateral force on the sample from the probe tip may cause damage to soft fragile samples. Tapping mode [9], [10] was developed to reduce lateral forces on such samples.

A schematic showing the typical instrumentation of an AFM operating in tapping mode is shown in Fig. 1. When operating in tapping mode, the cantilever probe is oscillated at one of its resonance frequencies, tapping the sample once every oscillation cycle while scanning. A piezoelectric stack actuator located at the base of the cantilever is typically used to oscillate the cantilever. New methods of actuation, such as electrostatic actuation [11] and coating the cantilever with piezoelectric material to act as a bimorph actuator, are being implemented to reduce the size of the AFM.

The magnitude of the cantilever oscillations in free air (A_0) is determined by the driving signal amplitude, the cantilever spring constant, and the quality (Q) factor of the cantilever's resonance. The magnitude of cantilever oscillations when tapping the sample $[A(t)]$ is typically measured using the optical lever method which involves reflecting a laser beam off the cantilever onto a photodiode sensor. Any change in position of the reflected laser spot on the sensor represents tip displacement. The ac signal obtained is then converted to a dc value using an rms-to-dc converter. This dc signal is sent to the Z-axis feedback controller (refer to Fig. 2) which controls the vertical

Manuscript received April 25, 2011; revised August 9, 2011; accepted August 29, 2011. Date of publication October 14, 2011; date of current version December 2, 2011. Subject Editor C. Mastrangelo.

The authors are with the School of Electrical Engineering and Computer Science, The University of Newcastle, Callaghan, NSW 2308, Australia (e-mail: Reza.Moheimani@newcastle.edu.au).

Color versions of one or more of the figures in this paper are available online at http://ieeexplore.ieee.org.

Digital Object Identifier 10.1109/JMEMS.2011.2168809

1057-7157/$26.00 © 2011 IEEE

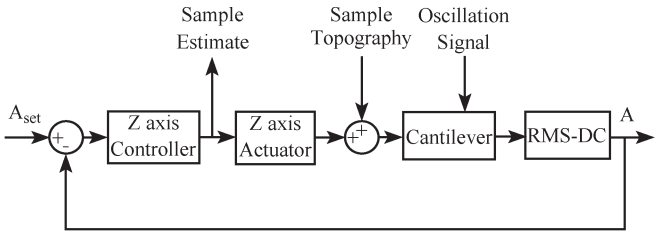

Fig. 2. Z-axis feedback control loop. The controller maintains the cantilever oscillation amplitude at the set point. The output of the controller provides an estimate of the sample topography.

distance between the cantilever base and the sample when scanning to maintain $A(t)$ at the set-point amplitude (A_{set}). To keep the tapping force on the sample to a minimum, A_{set} is chosen to be slightly less than A_0. As the probe is scanned across the sample, the feedback control signal provides an accurate representation of the sample topography.

As the tip is in intermittent contact with the sample, the lateral dragging forces are reduced, compared to contact-mode imaging [10], [12]. This has made tapping mode popular for imaging soft biological samples [12]–[14] and samples which are held loosely to their substrate.

Current commercially available AFMs are capable of imaging biological samples at a rate of 5 s per image frame which is too slow to observe dynamic biological processes which occur in milliseconds. The main limitation to scan speed when the AFM is operating in tapping mode is the speed of the Z-axis feedback loop. The faster the Z-axis feedback controller can respond to changes in the sample topography, the faster the sample may be scanned. The speed of the Z-axis feedback loop is limited by the bandwidth of the scanner in the Z-direction, the speed of the rms-to-dc converter, the error signal saturation, and the cantilever transient response.

The aim of this work is to present a new method of modifying the cantilever transient response which will enable increased scan speeds of an AFM operating in tapping mode. In Section II, the relationship between the cantilever transient response and the scan speed is discussed. The effect of piezoelectric shunt control on the cantilever Q factor is then analyzed in Section III. The design of a synthetic impedance for realization of piezoelectric shunt circuits is outlined in Section IV. Experimental results are presented in Section V, followed by conclusions and further work in Section VI.

II. Cantilever Transient Response

A. Q Factor Versus Scan Speed

To faithfully reproduce the sample topography, the response of the Z-axis feedback controller must be fast enough to ensure that the tip maintains contact with the sample. Ideally, when the sample contains a sharp drop, the error signal $(e(t) = A(t) - A_{\text{set}})$ of the feedback controller should have a magnitude that is proportional to the size of the drop. The slow transient response of the cantilever prevents this from happening. Fig. 3 shows the cantilever deflection when a sharp drop in the sample is encountered. When the drop is encountered, the tip loses contact with the sample. The transient response of the cantilever results in a delay before the error signal reaches its maximum value. The reduced error signal during this delay leads to a slower feedback response, increasing the time in which the tip is not in contact with the sample. Whenever the tip is not in contact with the sample, the sample topography cannot be recorded accurately. The increased time needed for the Z-axis feedback controller to respond to a sharp drop in the sample means that the scan speed must be reduced to maintain tip–sample contact.

To explain the difficulties related to transient response, the AFM cantilever may be modeled as a mass–spring–damper system. The equation of motion for a single mode is

$$m\ddot{d}(t) + b\dot{d}(t) + kd(t) = F(t) \tag{1}$$

where m is the effective mass of the cantilever, d is the vertical tip displacement, b is the damping coefficient, k is the spring constant, and $F(t)$ is the sum of external forces acting on the cantilever. In the Laplace domain, the transfer function from $F(s)$ to $D(s)$ is

$$\frac{D(s)}{F(s)} = \frac{\beta\omega_n^2}{s^2 + 2\zeta\omega_n s + \omega_n^2} \tag{2}$$

where ω_n is the natural frequency $(\omega_n = \sqrt{k/m})$, ζ is the damping ratio $(\zeta = b/2m\omega_n)$, and β is the steady-state gain.

The time response of (2) when $F(t)$ contains a step input will contain an exponentially decaying transient before reaching a steady-state value. In the case where the cantilever is being oscillated on a surface containing a sharp drop, as shown in Fig. 3, the time response of $e(t)$ is

$$e(t) = (A_0 - A_{\text{set}})(1 - e^{-\zeta\omega_n t}). \tag{3}$$

The rate at which $e(t)$ increases to reach its maximum value is determined by $\sigma = \zeta\omega_n$ (the distance of the poles from the imaginary axis). The further from the imaginary axis the poles lie, the faster $e(t)$ will increase. The parameter σ may be expressed in terms of the Q factor of the cantilever. Given that

$$Q = \frac{1}{2\zeta} \tag{4}$$

we may write

$$\sigma = \frac{\omega_n}{2Q}. \tag{5}$$

In a probe with a high Q factor, it will take longer for $e(t)$ to increase after a sharp drop in the sample topography, as shown in Fig. 3(a) and (b), resulting in slower scan speeds to accurately capture the sample topography. Scan speed may be increased by using a cantilever with a low Q factor or artificially reducing the Q factor of the cantilever.

B. Q Factor Versus Feedback Controller Gain

As the sample is scanned below the cantilever tip, the sample topography acts as a disturbance to the Z-axis feedback loop, as shown in Fig. 2. When the tracking error is low, the controller output is proportional to this disturbance and is

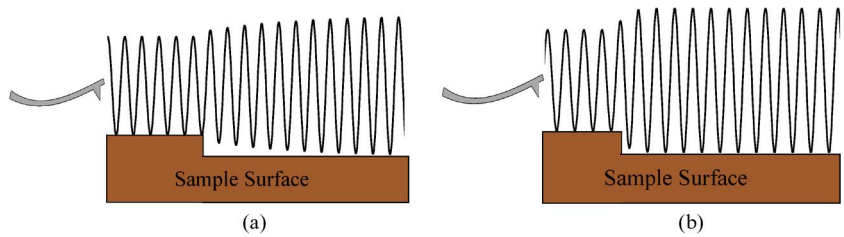

Fig. 3. Cantilever deflection as it is scanned over a sample with a sharp downward step, with the Z-axis feedback controller turned off. The cantilever with the lower Q factor responds faster to the change in sample topography. (a) High Q factor. (b) Low Q factor.

therefore used to represent the sample height when imaging. The response speed of the feedback loop to disturbances must be increased as the scan rate is increased in order to accurately track topographic features of the sample. Increasing the gain of the feedback loop will increase the response speed of the system. The feedback loop gain is limited by the gain margin of the loop. Increasing the gain margin of the feedback loop will allow for a higher controller gain and therefore improved image quality at higher scan rates.

In many AFMs, the Z-axis controller is an integral controller. The gain margin of the Z-axis feedback loop is determined by the transfer function of this integral controller in cascade with the transfer function from the cantilever input to the rms-to-dc converter output (A). Mertz *et al.* [15] modeled the transfer function from the cantilever input to the rms-to-dc converter output as a low-pass filter with a -3-dB frequency of

$$\Omega_{3\ \mathrm{dB}} = \frac{\omega_n}{2Q}. \tag{6}$$

The gain margin of the loop is increased by increasing $\Omega_{3\ \mathrm{dB}}$, which may be achieved by reducing the Q factor of the cantilever.

C. Q Factor Versus Tapping Force

The average tip–sample force (F_{TS}) is a function of the Q factor, A_{set}, and A_0 as shown by [16]

$$F_{\mathrm{TS}} \propto \frac{k}{Q}\sqrt{(A_0^2 - A_{\mathrm{set}}^2)}. \tag{7}$$

Reducing the cantilever Q factor, to increase the scan speed, will increase the tip–sample force, resulting in a reduction in the force sensitivity (image resolution) of the cantilever and an increase in the risk of damage to the sample. Maintaining A_0 close to A_{set} will reduce the tip–sample force. However, (3) shows that this will reduce the magnitude of the error signal sent to the Z-axis feedback controller.

Most AFM cantilevers designed for tapping mode have a higher Q factor than is needed for the desired resolution when scanning in air. To increase the scan speed, it is therefore desirable to decrease the Q factor of the cantilever. When scanning in liquid, the Q factor is significantly reduced by hydrodynamic forces. As a result, it may be desirable to increase the Q factor to increase the cantilever force sensitivity.

One developing application of the AFM is real-time imaging of biological processes. Ando *et al.* [17] have designed high-speed AFMs using new instrumentation and control techniques to observe processes such as the motion of myosin V molecules along an actin filament [18] and the structural changes occurring in bacteriorhodopsin when exposed to light [19]. To provide a sufficiently high scan rate for dynamic biological processes, the Q factor of the cantilever must be modified to suit the imaging environment.

D. Modification of the Cantilever Q Factor

Mertz *et al.* [15] developed a method of modifying the effective Q factor of an AFM cantilever probe termed "active Q control." This method has been used in some commercially available AFMs. The probe displacement signal measured by the photodiode sensor is phase shifted by $\pi/2$, to obtain the probe velocity. This velocity signal is then multiplied by a gain G and added to the probe actuation signal to modify the effective Q factor Q^* of the cantilever probe. The desired Q factor of the probe is set prior to scanning, by setting the value of G, to either increase the scan speed or reduce the tapping forces of the probe.

The equation of motion for a forced cantilever with an additional force $G\dot{d}(t)$ is

$$m\ddot{d}(t) + b\dot{d}(t) + kd(t) = F_0\cos(\omega_d t) + F_{\mathrm{TS}}(t) + G\dot{d}(t) \tag{8}$$

or equivalently

$$m\ddot{d}(t) + (b - G)\dot{d}(t) + kd(t) = F_0\cos(\omega_d t) + F_{\mathrm{TS}}(t) \tag{9}$$

where F_0 is the probe actuation signal amplitude, ω_d is the damped natural frequency of the probe $(\omega_d = \omega_n\sqrt{1-\zeta^2})$, and $F_{\mathrm{TS}}(t)$ is the force due to the tip–sample interaction. Equation (9) expressed in terms of ω_n and Q^* is

$$\ddot{d}(t) + \frac{\omega_n}{Q^*}\dot{d}(t) + \omega_n^2 d(t) = F_0\cos(\omega_d t) + F_{\mathrm{TS}}(t) \tag{10}$$

where

$$Q^* = \frac{m\omega_n}{(b - G)}. \tag{11}$$

Orun *et al.* [20] and Sahoo *et al.* [21] designed state feedback controllers based on the "active Q control" methodology which makes it possible to modify both ω_n and Q, allowing more freedom in obtaining the desired scan speed and image resolution.

The equation of motion for a forced cantilever with additional forces $G\dot{d}(t)$ and $Hd(t)$, where H is the displacement

feedback gain, is

$$m\ddot{d}(t) + b\dot{d}(t) + kd(t) = F_0 \cos(\omega_d t) + F_{\mathrm{TS}}(t) + G\dot{d}(t) + Hd(t) \quad (12)$$

or equivalently

$$m\ddot{d}(t) + (b-G)\dot{d}(t) + (k-H)d(t) = F_0 \cos(\omega_d t) + F_{\mathrm{TS}}(t). \quad (13)$$

Equation (13) expressed in terms of the effective natural frequency ω_n^* and Q^* is

$$\ddot{d}(t) + \frac{\omega_n^*}{Q^*}\dot{d}(t) + \omega_n^2 d(t) = F_0 \cos(\omega_d t) + F_{\mathrm{TS}}(t) \quad (14)$$

where

$$Q^* = \frac{m\omega_n^*}{(b-G)} \quad (15)$$

$$\omega_n^* = \sqrt{\frac{(k-H)}{m}}. \quad (16)$$

The method used to obtain velocity in *active Q control*, phase shifting of the displacement signal, introduces a time delay to the velocity signal and therefore cannot be used with the state feedback controller as both displacement and velocity are used by the controller. Sahoo *et al.* [21] used a state observer to obtain the velocity signal from the measured displacement signal.

Sahoo *et al.* [22] also introduced transient force AFM (TF-AFM). TF-AFM is a method of obtaining images with an AFM operating in tapping mode where the scan speed is not reliant on the Q factor of the cantilever probe. This method compares the output of an observer-based model of the cantilever to the output of the cantilever, and any difference between the model and the cantilever is measured and recorded. Any mismatch between the two outputs is due to the interaction between the probe and the sample, as the sample affects the cantilever but not the model. The difference in output between the model and the cantilever, due to sample interaction, occurs during transients, which means that there is no need to wait for the probe to achieve steady state.

The aforementioned methods have proven to be effective in obtaining the desired scan speed/resolution when operating in tapping mode. However, these control systems have several drawbacks as follows.

1) Implementation requires significant modification to the AFM.
2) The cantilever may be driven into unstable operation, leading to sample or tip damage.
3) The feedback signal relies on an optical sensor which is prone to noise.

The availability of self-actuating piezoelectric microcantilevers has made it possible to introduce a new technique of Q control that alleviates some of the aforementioned difficulties; this is discussed in the following.

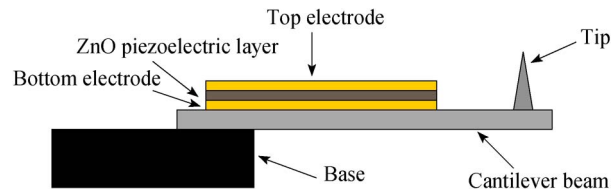

Fig. 4. Schematic of the DMASP microcantilever.

III. Passive Piezoelectric Shunt Control

The ability of piezoelectric materials to transform mechanical energy into electrical energy and vice versa has led to their use in damping undesired vibration in flexible structures such as snowboards [23], automobile bodies [24], flexible space structures [25], and aircraft [26]. Piezoelectric shunt damping involves bonding a piezoelectric transducer to a structure and connecting an electrical impedance to its terminals [27]. Shunt damping was first introduced by Forward [28] with an experimental demonstration of the technique. An analytical description of shunt damping was later presented by Hagood and von Flotow [29] in which the shunt circuit is shown to be analogous to a mechanical proof mass damper.

Piezoelectric shunt damping has been used to increase the bandwidth of AFM scanners by damping the first resonant mode of the scanner. This was demonstrated in [30] and [31] with a piezoelectric tube scanner and in [32] with a piezoelectric-stack-actuated flexure-based scanner.

The aim of this work is to show that the technique of piezoelectric shunt control is an effective way of modifying the Q factor of a piezoelectric AFM microcantilever. Passive piezoelectric shunt control has several advantages as follows.

1) When the shunt impedance is passive, system stability is ensured.
2) Feedback sensors are not required; therefore, the measurement noise and bandwidth constraints of optical sensors are avoided.
3) The system implementation is inexpensive, and minimal modification is required to existing microscopes.

The microcantilever used in this work is the DMASP AFM microcantilever available from Bruker AFM Probes [33]. A schematic of the DMASP cantilever is shown in Fig. 4. The cantilever has a length of 120 μm and a width of 55 μm with a thin layer of piezoelectric ZnO material deposited on the bottom surface. A layer of Ti/Au is bonded above and below the ZnO layer acting as electrodes. Applying a voltage to the electrodes causes the piezoelectric layer to expand or contract, depending on the polarity of the voltage, resulting in flexure of the cantilever. A sinusoidal voltage is applied to the electrodes to oscillate the cantilever tip when operating in tapping mode. The piezoelectric transducer may be modeled as a strain-dependent voltage source v_p in series with a capacitance C_p [34]. When a shunt impedance $Z(s)$, consisting of a resistor R and an inductor L, is placed in series with the driving voltage source v_s, an LRC circuit is obtained, as shown in Fig. 5. This LRC circuit is tuned to the mechanical resonance of the cantilever, resulting in a damped electrical resonance, which decreases the Q factor of the probe. Varying the value of R in

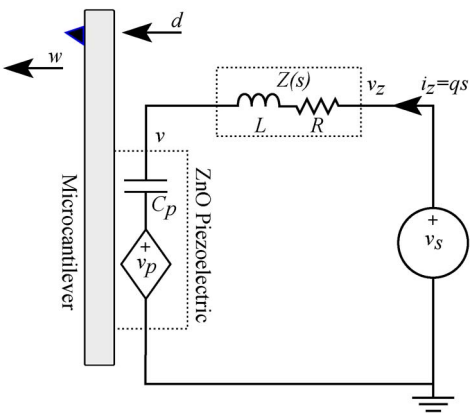

Fig. 5. Piezoelectric AFM microcantilever with attached shunt circuit.

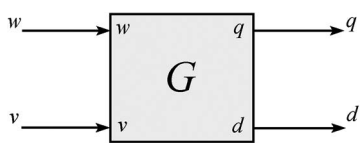

Fig. 6. Piezoelectric cantilever model describing the tip displacement (d) and the generated charge (q) in response to an applied voltage (v) and disturbance (w).

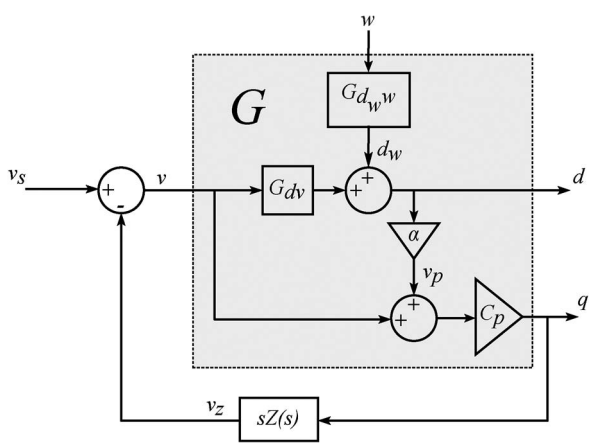

Fig. 7. Block diagram of the shunted system.

the circuit will vary the amount of electrical damping; therefore, the probe Q factor may be tuned by varying the value of R in the circuit.

A. System Modeling

The piezoelectric cantilever may be modeled by the system G, as shown in Fig. 6, where w is a disturbance strain on the cantilever due to a change in the sample topography, d is the displacement of the cantilever tip, v is the voltage across the piezoelectric transducer terminals, and q is the charge generated by the piezoelectric transducer. The electrical and mechanical system shown in Fig. 5 may be represented by the block diagram in Fig. 7, where v_z is the voltage across the shunt impedance, α is the actuator voltage-to-displacement coefficient $(\alpha = v_p/d)$, d_w is the initial displacement due to a sample perturbation, $G_{dv}(s)$ is the transfer function from $v(s)$ to $d(s)$, and $G_{d_w w}(s)$ is the transfer function from $\omega(s)$ to $d_w(s)$. In the standard second-order transfer function form

$$G_{dv}(s) = \frac{d(s)}{v(s)} = \frac{\beta_v \omega_n^2}{s^2 + 2\zeta\omega_n s + \omega_n^2} \tag{17}$$

$$G_{d_w w}(s) = \frac{d_w(s)}{w(s)} = \frac{\beta_w \omega_n^2}{s^2 + 2\zeta\omega_n s + \omega_n^2} \tag{18}$$

where β_v and β_w are the steady-state gains of $G_{dv}(s)$ and $G_{d_w w}(s)$, respectively.

B. Modeling the Transfer Function From Actuating Voltage to Tip Displacement

From the block diagram in Fig. 7, the transfer function from v_s to v may be derived as

$$G_{vv_s}(s) = \frac{v(s)}{v_s(s)} = \frac{1}{1 + sZ(s)G_{qv}(s)} \tag{19}$$

where $G_{qv}(s)$ is the transfer function from $v(s)$ to $q(s)$ represented by

$$G_{qv}(s) = \frac{q(s)}{v(s)} = \alpha C_p G_{dv} + C_p. \tag{20}$$

Substituting (20) into (19), we obtain the transfer function from $v_s(s)$ to $v(s)$

$$G_{vv_s}(s) = \frac{\frac{1}{1+sZ(s)C_p}}{1 + \frac{sZ(s)C_p\alpha G_{dv}(s)}{1+sZ(s)C_p}}. \tag{21}$$

To simplify (21), let

$$H(s) = \frac{1}{1 + sZ(s)C_p} \tag{22}$$

$$K(s) = \frac{sZ(s)C_p\alpha}{1 + sZ(s)C_p} \tag{23}$$

then

$$G_{vv_s}(s) = \frac{H(s)}{1 + K(s)G_{dv}(s)}. \tag{24}$$

The transfer function from v_s to d, when the shunt is applied, is now found to be

$$G_{dv_s}(s) = G_{vv_s}(s)G_{dv}(s) = \frac{H(s)G_{dv}(s)}{1 + K(s)G_{dv}(s)}. \tag{25}$$

G_{dv_s} may be viewed as a negative feedback loop with a filter $H(s)$ (which is due to the electrical dynamics of the shunt impedance) in the feedforward path as shown in Fig. 8. $H(s)$ adds a filter in the cantilever transfer function from v_s to d. For accurate tracking, the driving signal must be prefiltered by $H^{-1}(s)$ to compensate for $H(s)$. When operating in tapping mode, the driving signal is a single frequency sinusoid. The effect of $H(s)$ on this signal is a modification of magnitude and phase. The change in magnitude can easily be compensated for by varying the amplitude of the drive signal. The change in

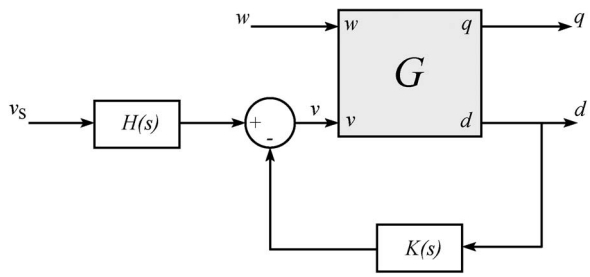

Fig. 8. Equivalent feedback system from v_s to d.

phase will not affect the operation of the device, so there is no need to compensate for this.

C. Modeling the Transfer Function From a Perturbation in Sample Topography to Tip Displacement

To obtain the transfer function from a perturbation in sample topography to the tip displacement, $v_s(s)$ is first set to zero. From Fig. 7, it is observed that

$$v = -v_z(s) \tag{26}$$
$$v_z(s) = sq(s)Z(s) \tag{27}$$

where $q(s)$ is given by

$$q(s) = -v_z(s)C_p - v_z(s)\alpha C_p G_{dv}(s) + d_w(s)\alpha C_p. \tag{28}$$

Substituting (28) into (27) gives

$$v_z(s) = (-v_z(s)C_p - v_z(s)\alpha C_p G_{dv}(s) + d_w(s)\alpha C_p)\, sZ(s). \tag{29}$$

Substituting (26) into (29) results in the transfer function

$$G_{vd_w}(s) = \frac{v(s)}{d_w(s)} = \frac{-\alpha sZ(s)C_p}{1 + sZ(s)C_p + \alpha sZ(s)C_p G_{dv}(s)}. \tag{30}$$

From Fig. 7, it is observed that

$$d(s) = G_{vd_w}(s)G_{dv}(s)d_w(s) + d_w(s). \tag{31}$$

Substituting (30) into (31) results in the transfer function

$$G_{dd_w}(s) = \frac{d(s)}{d_w(s)} = \frac{1}{1 + \frac{\alpha sZ(s)C_p G_{dv}(s)}{1+sZ(s)C_p}} = \frac{1}{1 + K(s)G_{dv}(s)}. \tag{32}$$

Combining (32) and (18) results in the transfer function

$$G_{dw}(s) = G_{dd_w}(s)G_{d_w w}(s) = \frac{G_{d_w w}(s)}{1 + K(s)G_{dv}(s)}. \tag{33}$$

Note that the transfer function $G_{d_w w}(s)$ has the same poles as $G_{dv}(s)$, with the only difference being the steady-state gain β_w. The transfer function $G_{dw}(s)$ may be written as

$$G_{dw}(s) = \frac{\lambda G_{dv}(s)}{1 + K(s)G_{dv}(s)} \tag{34}$$

as shown in Fig. 9, where $\lambda = \beta_w/\beta_v$. Therefore, it can be seen that the transfer function from a perturbation in the sample topography to the tip displacement may be viewed as a negative feedback system. The controller $K(s)$ may be designed using standard feedback control techniques, allowing the poles of $G_{dw}(s)$ to be placed according to the desired performance objectives.

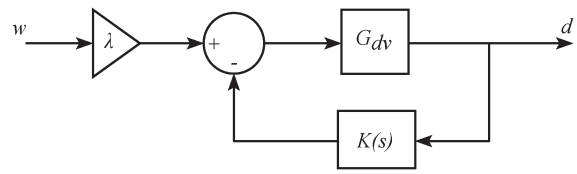

Fig. 9. Feedback interpretation transfer function from disturbance to displacement.

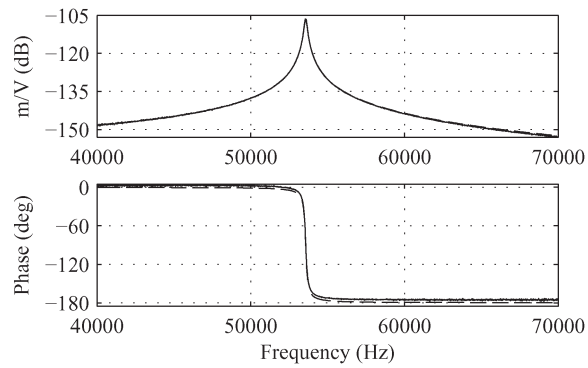

Fig. 10. Frequency response of (- -) the first cantilever mode and (—) the fitted model.

D. System Model Parameters Obtained From Experimental Results

To determine the optimal values for L and R, mathematical models of $G_{dv}(s)$ and $K(s)$ must be obtained and analyzed. A frequency response of $G_{dv}(s)$ was obtained by using a microscope scanning laser Doppler vibrometer (Polytec MSV 400). The cantilever was excited by applying a pseudorandom signal, and the resulting tip displacement was measured. The frequency response of $G_{dv}(s)$ is shown in Fig. 10. A mathematical model of $G_{dv}(s)$ obtained by system identification is also shown in Fig. 10.

Note from (23) that α and C_p are properties of the cantilever and must be determined in order to design $K(s)$. C_p was measured at 23 pF using an Agilent E4980A LCR meter. The value of α was determined by measuring the frequency response of the admittance $G_{iv}(s)$ and obtaining a model through system identification. Rearranging (20) results in the transfer function

$$G_{iv}(s) = \frac{i(s)}{v(s)} = \frac{q(s)s}{v(s)} = \alpha C_p G_{dv}(s)s + C_p s. \tag{35}$$

The only unknown in (35) is α which was obtained by equating (35) to the model obtained through system identification. $\alpha \approx 2 \times 10^4$.

E. Optimal Shunt Impedance Parameters

1) Inductance: For a series LCR circuit, the undamped resonance frequency is given by

$$\omega_r = 2\pi f_r = 1/\sqrt{LC_p}. \tag{36}$$

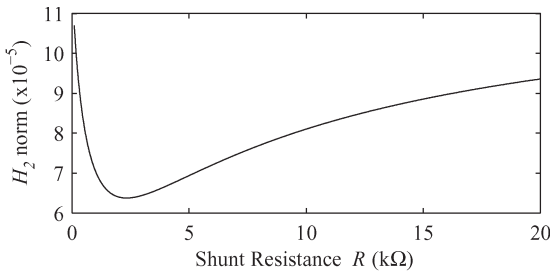

Fig. 11. H_2 norm of G_{dw} versus R.

From the frequency response shown in Fig. 10, it can be seen that the resonance frequency (f_r) of the first mode occurs at 53 580 Hz. Note that the resonance frequency will change from f_r to f_d when the shunt circuit is connected, altering the required value of L. As the Q factor is significantly high, it may be assumed that $f_d \approx f_r$; therefore, the change in L will be insignificant. Substituting the values for f_r and C_p into (36) gives a value for L of 377 mH.

2) Resistance: The H_2 norm of the transfer function $G_{dw}(s)$ was used to determine the lowest Q factor which can be obtained with the DMASP cantilever using passive piezoelectric shunt control. The H_2 norm of a system represents the variance of the output given a white-noise input. When the H_2 norm of the system is minimized, the system damping is at a maximum since the area under the magnitude curve of the frequency response is minimized. The H_2 norm of $G_{dw}(s)$ was obtained using the command `norm` in Matlab. A plot of the H_2 norm of $G_{dw}(s)$ for a varying resistance is shown in Fig. 11. From the plot, it can be seen that the value of R which minimizes the H_2 norm is $R = 2335\ \Omega$. Using this value of R in the shunt impedance will give the minimal Q factor obtainable using passive shunt control.

IV. Synthetic Impedance

The resonance modes of the cantilever may change with environmental conditions (for example, temperature and air pressure). The resonance modes will also differ from cantilever to cantilever due to manufacturing tolerances and material imperfections. It is therefore desirable to be able to fine tune the parameters of the impedance online. Implementing synthetically the shunt impedance allows online fine tuning of shunt impedance parameters.

An arbitrary impedance $Z(s)$ may be implemented synthetically [35] by measuring the terminal voltage $v_z(s)$ and controlling the terminal current $i_z(s)$ according to the relationship $v_z(s)/i_z(s) = Z(s)$ or $i_z(s) = v_z(s)Y(s)$.

A simple RC filter and a voltage-controlled current source, as shown in Fig. 12, are used to implement an impedance $Z(s) = Ls + R$. The complete circuit in Fig. 12 is equivalent to the shunt impedance circuit shown in Fig. 5. From Fig. 12, it is observed that

$$\frac{v_{\text{out}}(s)}{v_z(s)} = \frac{1}{R_f C_f s + 1} \tag{37}$$

$$i_z(s) = \frac{v_{\text{out}}(s)}{R_c}. \tag{38}$$

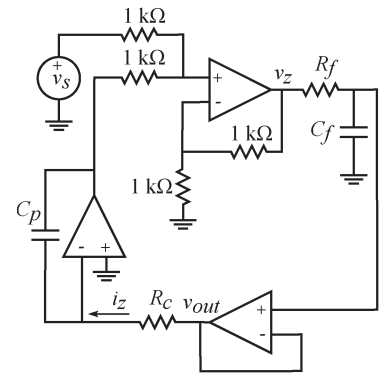

Fig. 12. LRC circuit implemented with a synthetic impedance.

The resulting impedance is now found to be

$$Z(s) = \frac{v_z}{i(s)} = \frac{v_z(s)R_c}{v_{\text{out}}(s)} = R_c R_f C_f s + R_c \tag{39}$$

where

$$L = R_c R_f C_f \tag{40}$$

$$R = R_c. \tag{41}$$

By varying R_c and R_f, using potentiometers, the values of L and R may be modified accordingly.

The operational amplifiers used in the circuit are Linear Technology LT1468 operational amplifiers [36]. This operational amplifier was chosen due to its high gain–bandwidth product (90 MHz) and its low input bias current (10 nA).

V. Experimental Results

To test the effectiveness of the shunt, the frequency response and the step response of $G_{dw}(s)$ are desired. To test $G_{dw}(s)$, a piezoelectric shaker is placed under the cantilever, and the response was observed with the Polytec MSV 400. Two problems arose when undertaking these experiments as follows.

1) The mounting on which the cantilever was placed added additional dynamics to the system.
2) It is difficult to find a shaker with resonance modes higher than those of the DMASP microcantilever, to ensure that these resonances do not affect the measurement.

Due to the difficulties encountered when obtaining the frequency response of the transfer function $G_{dw}(s)$, $G_{dv_s}(s)$ was used as a performance indicator.

Equation (25) shows that $G_{dv_s}(s) = H(s)G_{dv}(s)/1 + K(s)G_{dv}(s)$, and (34) shows that $G_{dw}(s) = \lambda G_{dv}(s)/1 + K(s)G_{dv}(s)$. Equating (25) and (34) gives

$$G_{dw}(s) = \lambda H(s)^{-1} G_{dv_s}(s) \tag{42}$$

where

$$H(s)^{-1} = 1 + sZC_p = s^2 + \frac{Rs}{L} + \frac{1}{LC_p}. \tag{43}$$

Therefore, to test the effectiveness of the shunt-controlled system on $G_{dw}(s)$, it is sufficient to test $H(s)^{-1}G_{dv_s}(s)$. Note that

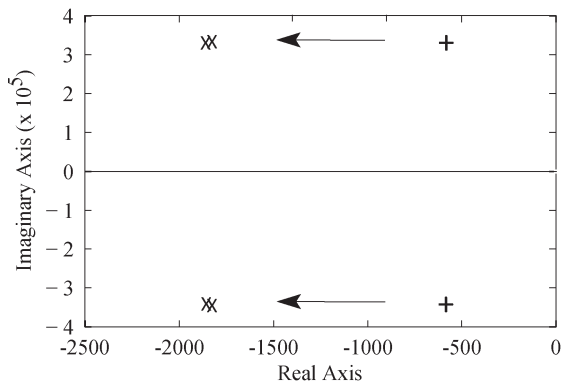

Fig. 13. (+) Open- and (x) closed-loop pole locations of the piezoelectric-shunt-controlled cantilever.

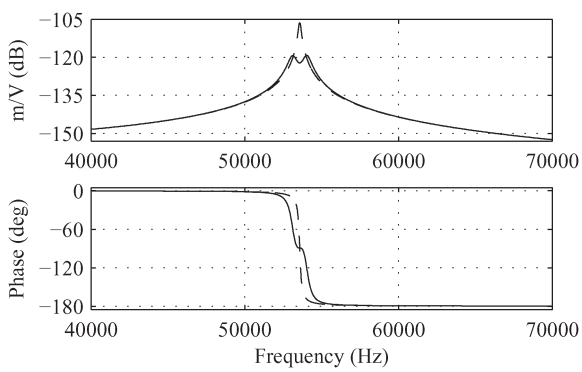

Fig. 14. Frequency response of (- -) $G_{dv_s}(s)$ with the cantilever in open loop and (—) $H(s)^{-1}G_{dv_s}(s)$ with the cantilever in closed loop. A reduction of 13 dB in the resonance peak can be observed.

the gain λ will have no effect on the closed-loop poles of the system, so it can be ignored.

The synthetic impedance consisting of a voltage-controlled current source and a passive RC filter, as shown in Fig. 12, was used to implement $Z(s)$. The input $v_s(s)$ was prefiltered by $H(s)^{-1}$ before being applied to the circuit. The Polytec MSV 400 was used to obtain the frequency response and the step response of $H(s)^{-1}G_{dv_s}(s)$.

Fig. 13 shows the open- and closed-loop pole locations of the cantilever. It is clear from this figure that the introduction of the shunt impedance has significantly shifted the poles of the cantilever further into the left half-plane, increasing the damping of the cantilever. Fig. 14 shows the frequency response plot of $G_{dv_s}(s)$ with the cantilever in open loop and $H(s)^{-1}G_{dv_s}(s)$ with the cantilever in closed loop. A 13-dB reduction of the resonance peak is observed from open loop to closed loop.

The response of $G_{dv_s}(s)$ to a step of 2.6 V with the cantilever in open loop is shown in Fig. 15, and the step response of $H(s)^{-1}G_{dv_s}(s)$ with the cantilever in closed loop is shown in Fig. 16. It can be seen that the addition of the shunt impedance has reduced the settling time from 9 to 2 ms.

This reduction in transient settling time of 7 ms means that the scan speed of the AFM may be increased without distorting the image obtained.

The effective Q factor of the cantilever probe may be determined from an analysis of the step response. Note from (5) that the exponential decay rate is $\sigma = \omega_n/2Q$. The exponential decay rate may be defined as the time taken for the step response to decay to 36.79% of its peak amplitude. ω_n is measured from the frequency response in Fig. 14, and σ is measured from the step responses in Figs. 15 and 16. The effective Q factor with the cantilever in open and closed loops can now be calculated from (5). A reduction in the effective Q factor from 297.6 in open loop to 35.5 in closed loop was observed.

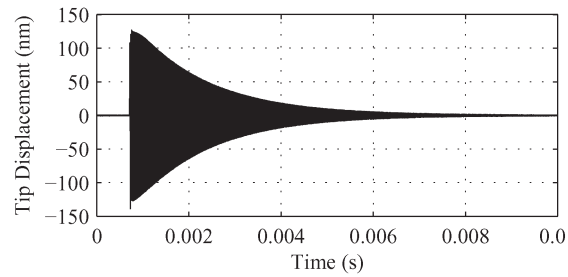

Fig. 15. Step response of $G_{dv_s}(s)$ in open loop.

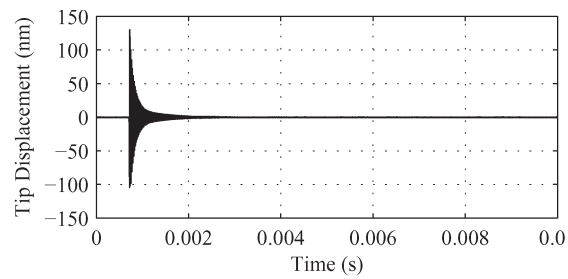

Fig. 16. Step response of $H(s)^{-1}G_{dv_s}(s)$ in closed loop.

Images of an NT-MDT TGZ1 [37] calibration grating were obtained with an NT-MDT NTEGRA AFM [37] that was instrumented with the Q-controlled microcantilever. The NT-MDT TGZ1 calibration grating consists of a periodic step formed from silicon dioxide with a period of 3 ± 0.05 μm and a step height of 18.5 ± 1 nm.

Scans were obtained with the damped and undamped cantilevers on a 10 μm $\times$ 10 μm section of the calibration grating at a scan speed of 20 μm/s. The Z-axis feedback controller gain (K_I) was increased until the loop became unstable. K_I was then reduced slightly to ensure loop stability. The maximum value of K_I obtainable using the undamped cantilever was 0.02 compared to a value of 0.2 using the damped cantilever. This increase in feedback gain by a factor of ten significantly reduced the distortion of the image obtained, as shown in Fig. 17. This demonstrates that piezoelectric shunt control can significantly improve the Z-axis feedback bandwidth, which improves the image quality or imaging speed.

VI. Conclusion/Further Work

When using tapping mode to obtain an image of a sample, it may be desired to modify the Q factor of the cantilever according to the sample being imaged and the imaging environment. Reducing the Q factor of the cantilever will enable an increase in scan speed. Increasing the Q factor of the cantilever will reduce the tip–sample interaction force, resulting in increased force sensitivity and a reduction in the risk of sample damage.

Passive piezoelectric shunt control is presented in this work as a new method for reducing the Q factor of a self-actuating

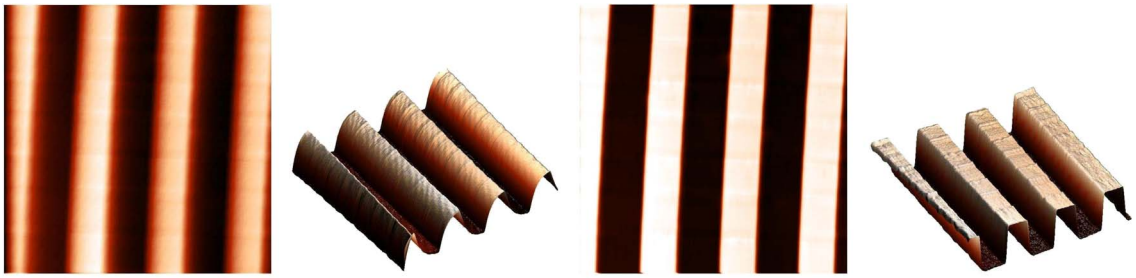

(a) (b) (c) (d)

Fig. 17. Images of the NT-MDT TGZ1 calibration grating obtained at a scan speed of 20 μm/s. In each case, the maximum value of K_I, which ensured loop stability, was used. The use of piezoelectric shunt control to damp the cantilever increased the cantilever response speed and allowed a higher feedback gain and, consequently, reduced image distortion. (a) Two-dimensional image without shunt control. (b) Three-dimensional image without shunt control. (c) Two-dimensional image with shunt control. (d) Three-dimensional image with shunt control.

piezoelectric AFM microcantilever. It has been shown that a passive shunt impedance can reduce the effective Q factor by a factor of eight. This results in an improvement of either image quality or scan speed.

It is shown that the transfer function from a disturbance, due to a sample feature, to tip displacement is equivalent to a negative feedback loop when a shunt impedance is added to the cantilever oscillation circuit. This representation allows the use of standard control design techniques to place the poles of the shunted microcantilever in arbitrary locations to achieve desired performance objectives.

Increasing the Q factor of the cantilever, to increase force sensitivity and reduce the risk of sample damage, is not possible with a passive impedance. If an increase in Q factor is required, an active impedance [38] may be designed using techniques such as the pole-placement method to increase the Q factor. There is a limit on how far the Q factor of the cantilever may be minimized using a passive shunt circuit. The use of an active impedance will also allow further reductions in the Q factor of the cantilever. The authors are currently working on the implementation of an active impedance using a field-programmable analog array (FPAA).

Future work includes reducing error saturation [39] through adaptive shunt control [40], [41]. Error saturation occurs when the tip loses contact with the sample after the cantilever approaches a sharp drop in the sample and the cantilever oscillation amplitude reaches its free-air limit of A_0 before the Z-axis feedback controller can restore the tip–sample contact. This means that the feedback error signal has saturated, reducing the response time of the scanner in the vertical direction, resulting in a distorted image. Momentarily increasing the probe Q factor when saturation occurs will lead to an increase in A_0, preventing error saturation [42]. By implementing shunt control with an FPAA, it will be possible to switch the shunt impedance with a short circuit when A approaches A_0. This will momentarily increase A_0, allowing a higher feedback error signal, therefore reducing distortion in the image.

REFERENCES

[1] G. Binnig, C. F. Quate, and C. Gerber, "Atomic force microscope," *Phys. Rev. Lett.*, vol. 56, no. 9, pp. 930–933, Mar. 1986.

[2] S. A. C. Gould, B. Drake, C. B. Prater, A. L. Weisenhorn, S. Manne, H. G. Hansma, P. K. Hansma, J. Massie, M. Longmire, V. Elings, B. D. Northern, B. Mukergee, C. M. Peterson, W. Stoeckenius, T. R. Albrecht, and C. F. Quate, "From atoms to integrated circuit chips, blood cells, and bacteria with the atomic force microscope," *J. Vac. Sci. Technol. A, Vac. Surf. Films*, vol. 8, no. 1, pp. 369–373, Jan. 1990.

[3] S. Manne, H. J. Butt, S. A. C. Gould, and P. K. Hansma, "Imaging metal atoms in air and water using the atomic force microscope," *Appl. Phys. Lett.*, vol. 56, no. 18, pp. 1758–1759, Apr. 1990.

[4] D. Fotiadis, S. Scheuring, S. A. Muller, A. Engel, and D. J. Muller, "Imaging and manipulation of biological structures with the AFM," *Micron*, vol. 33, no. 4, pp. 385–397, Jan. 2002.

[5] N. Oyabu, O. Custance, I. Yi, Y. Sugawara, and S. Morita, "Mechanical vertical manipulation of selected single atoms by soft nanoindentation using near contact atomic force microscopy," *Phys. Rev. Lett.*, vol. 90, no. 17, p. 176 102, May 2003.

[6] J. Loos, "The art of SPM: Scanning probe microscopy in materials science," *Adv. Mater.*, vol. 17, no. 15, pp. 1821–1833, Aug. 2005.

[7] O. H. Willemsen, M. M. Snel, A. Cambi, J. Greve, B. G. D. Grooth, and C. G. Figdor, "Biomolecular interactions measured by atomic force microscopy," *Biophys. J.*, vol. 79, no. 6, pp. 3267–3281, Dec. 2000.

[8] S. Kasas, N. H. Thomson, B. L. Smith, P. K. Hansma, J. Miklossy, and H. G. Hansma, "Biological applications of the AFM: From single molecules to organs," *Int. J. Imag. Syst. Technol.*, vol. 8, no. 2, pp. 151–161, 1997.

[9] R. Garca and R. Prez, "Dynamic atomic force microscopy methods," *Surf. Sci. Rep.*, vol. 47, no. 6–8, pp. 197–301, Sep. 2002.

[10] Q. Zhong, D. Inniss, K. Kjoller, and V. Elings, "Fractured polymer/silica fiber surface studied by tapping mode atomic force microscopy," *Surf. Sci.*, vol. 290, no. 1/2, pp. L688–L692, Jun. 1993.

[11] P. Agarwal, D. Sahoo, A. Sebastian, H. Pozidis, and M. Salapaka, "Real-time models of electrostatically actuated cantilever probes with integrated thermal sensor for nanoscale interrogation," *J. Microelectromech. Syst.*, vol. 19, no. 1, pp. 83–98, Feb. 2010.

[12] A. S. Paulo and R. Garca, "High-resolution imaging of antibodies by tapping-mode atomic force microscopy: Attractive and repulsive tip–sample interaction regimes," *Biophys. J.*, vol. 78, no. 3, pp. 1599–1605, Mar. 2000.

[13] S. Kasas, N. H. Thomson, B. L. Smith, H. G. Hansma, X. Zhu, M. Guthold, C. Bustamante, E. T. Kool, M. Kashlev, and P. K. Hansma, "Escherichia coli RNA polymerase activity observed using atomic force microscopy," *Biochemistry*, vol. 36, no. 3, pp. 461–468, Jan. 1997.

[14] P. Parot, Y. F. Dufrne, P. Hinterdorfer, C. L. Grimellec, D. Navajas, J.-L. Pellequer, and S. Scheuring, "Past, present and future of atomic force microscopy in life sciences and medicine," *J. Mol. Recognit.*, vol. 20, no. 6, pp. 418–431, Nov./Dec. 2007.

[15] J. Mertz, O. Marti, and J. Mlynek, "Regulation of a microcantilever response by force feedback," *Appl. Phys. Lett.*, vol. 62, no. 19, pp. 2344–2346, May 1993.

[16] T. R. Rodriguez and R. Garcia, "Theory of Q control in atomic force microscopy," *Appl. Phys. Lett.*, vol. 82, no. 26, pp. 4821–4823, Jun. 2003.

[17] T. Ando, T. Uchihashi, and T. Fukuma, "High-speed atomic force microscopy for nano-visualization of dynamic biomolecular processes," *Progr. Surf. Sci.*, vol. 83, no. 7–9, pp. 337–437, Nov. 2008.

[18] N. Kodera, D. Yamamoto, R. Ishikawa, and T. Ando, "Video imaging of walking myosin V by high-speed atomic force microscopy," *Nature*, vol. 468, no. 7320, pp. 72–76, Nov. 2010.

[19] M. Shibata, H. Yamashita, T. Uchihashi, H. Kandori, and T. Ando, "High-speed atomic force microscopy shows dynamic molecular processes in photoactivated bacteriorhodopsin," *Nat. Nanotechnol.*, vol. 5, no. 3, pp. 208–212, 2010.

[20] B. Orun, S. Necipoglu, C. Basdogan, and L. Guvenc, "State feedback control for adjusting the dynamic behavior of a piezoactuated bimorph atomic force microscopy probe," *Rev. Sci. Instrum.*, vol. 80, no. 6, p. 063701, Jun. 2009.
[21] D. R. Sahoo, T. De Murti, and V. Salapaka, "Observer based imaging methods for atomic force microscopy," in *Proc. 44th IEEE CDC-ECC*, 2005, pp. 1185–1190.
[22] D. R. Sahoo, P. Agarwal, and M. V. Salapaka, "Transient force atomic force microscopy: A new nano-interrogation method," in *Proc. ACC*, 2007, pp. 2135–2140.
[23] E. Bianchini, R. Spangler, and C. Andrus, "The use of piezoelectric devices to control snowboard vibrations," in *Proc. SPIE Smart Struct. Mater.: Smart Struct. Integr. Syst.*, 1998, p. 106 114.
[24] L. Lecce, F. Franco, B. Maja, G. Montouri, and N. Zandonella, "Vibration active control inside a car by using piezo actuators and sensors," in *Proc. 28th Int. Symp. Autom. Technol. Autom.*, 1995, pp. 423–432.
[25] N. W. Hagood and E. F. Crawley, "Experimental investigation of passive enhancement of damping for space structures," *AIAA J. Guid. Navig. Control*, vol. 14, no. 6, pp. 1100–1109, 1991.
[26] J. Simpson and J. Schweiger, "An industrial approach to piezo electric damping of large fighter aircraft components," in *Proc. Ind. Commer. Appl. Smart Struct. Technol.*, San Diego, CA, 1998, pp. 34–46.
[27] S. O. R. Moheimani, "A survey of recent innovations in vibration damping and control using shunted piezoelectric transducers," *IEEE Trans. Control Syst. Technol.*, vol. 11, no. 4, pp. 482–494, Jul. 2003.
[28] R. L. Forward, "Electronic damping of vibrations in optical structures," *Appl. Opt.*, vol. 18, no. 5, pp. 690–697, Mar. 1979.
[29] N. W. Hagood and A. von Flotow, "Damping of structural vibrations with piezoelectric materials and passive electrical networks," *J. Sound Vib.*, vol. 146, no. 2, pp. 243–268, Apr. 1991.
[30] A. J. Fleming and S. O. R. Moheimani, "Sensorless vibration suppression and scan compensation for piezoelectric tube nanopositioners," *IEEE Trans. Control Syst. Technol.*, vol. 14, no. 1, pp. 33–44, Jan. 2006.
[31] S. Aphale, A. J. Fleming, and S. O. R. Moheimani, "High speed nanoscale positioning using a piezoelectric tube actuator with active shunt control," *Micro Nano Lett.*, vol. 2, no. 1, pp. 9–12, Mar. 2007.
[32] A. A. Eielsen and A. J. Fleming, "Passive shunt damping of a piezoelectric stack nanopositioner," in *Proc. Amer. Control Conf.*, Baltimore, MD, Jun. 2010, pp. 4963–4968.
[33] *Bruker AFM Probes Website*, 2010. [Online]. Available: http://www.brukerafmprobes.com/p-3252-dmasp.aspx
[34] J. J. Dosch, D. J. Inman, and E. Garcia, "A self-sensing piezoelectric actuator for collocated control," *J. Intell. Mater. Syst. Struct.*, vol. 3, no. 1, pp. 166–185, Jan. 1992.
[35] A. J. Fleming, S. Behrens, and S. O. R. Moheimani, "Synthetic impedance for implementation of piezoelectric shunt damping circuits," *Electron. Lett.*, vol. 36, no. 18, pp. 1525–1526, Aug. 2000.
[36] *Linear Technology Website*, 2010. [Online]. Available: http://www.linear.com
[37] *NT-MDT Website*, 2011. [Online]. Available: http://www.ntmdt.com
[38] A. J. Fleming and S. O. R. Moheimani, "Control oriented synthesis of high performance piezoelectric shunt impedances for structural vibration control," *IEEE Trans. Control Syst. Technol.*, vol. 13, no. 1, pp. 98–112, Jan. 2005.
[39] T. Sulchek, G. G. Yaralioglu, C. F. Quate, and S. C. Minne, "Characterization and optimization of scan speed for tapping-mode atomic force microscopy," *Rev. Sci. Instrum.*, vol. 73, no. 8, pp. 2928–2936, Aug. 2002.
[40] A. J. Fleming and S. O. R. Moheimani, "Adaptive piezoelectric shunt damping," *Smart Mater. Struct.*, vol. 12, no. 1, pp. 36–48, Feb. 2003.
[41] D. Niederberger, A. J. Fleming, S. O. R. Moheimani, and M. Morari, "Adaptive multimode resonant piezoelectric shunt damping," *Smart Mater. Struct.*, vol. 13, no. 5, pp. 1025–1035, Oct. 2004.
[42] I. Gunev, A. Varol, S. Karaman, and C. Basdogan, "Adaptive *Q* control for tapping-mode nanoscanning using a piezoactuated bimorph probe," *Rev. Sci. Instrum.*, vol. 78, no. 4, pp. 043707-1–043707-1, Apr. 2007.

Matthew W. Fairbairn (S'11) was born in Newcastle, Australia. He received the B.E.E. degree from The University of Newcastle, Callaghan, Australia, in 2009, where he is currently working toward the Ph.D. degree in electrical engineering.

His research interests include the limitations of high-speed atomic force microscopy due to piezoelectric actuator and cantilever dynamics.

S. O. Reza Moheimani (F'11) received the B.Sc. degree in electrical and electronics engineering from Shiraz University, Shiraz, Iran, in 1990, the M.Eng.Sc. degree from The University of New South Wales (UNSW), Sydney, Australia, in 1993, and the Ph.D. degree in electrical engineering from UNSW, Canberra, Australia, in 1996.

He joined The University of Newcastle, Callaghan, Australia, in 1997, where he founded and directs the Laboratory for Dynamics and Control of Nanosystems, a multimillion-dollar state-of-the-art research facility dedicated to the advancement of nanotechnology through innovations in systems and control engineering. He is a Professor and an Australian Research Council Future Fellow with the School of Electrical Engineering and Computer Science, The University of Newcastle. He has held several visiting appointments at the IBM Zurich Research Laboratory. His current research interests are mainly in the area of dynamics and control at the nanometer scale and include applications of control and estimation in nanopositioning systems for high-speed scanning probe microscopy, modeling and control of microcantilever-based devices, control of electrostatic microactuators in microelectromechanical systems, and control issues related to ultrahigh-density probe-based data storage systems.

Prof. Moheimani is a Fellow of the International Federation of Automatic Control and the Institute of Physics (U.K.). He was a corecipient of the 2007 IEEE TRANSACTIONS ON CONTROL SYSTEMS TECHNOLOGY Outstanding Paper Award and the 2009 IEEE Control Systems Society Control Systems Technology Award, together with a group of researchers from the IBM Zurich Research Laboratory. He has served on the Editorial Boards of a number of journals, including the IEEE TRANSACTIONS ON CONTROL SYSTEMS TECHNOLOGY, the IEEE/ASME TRANSACTIONS ON MECHATRONICS, and *Control Engineering Practice*, and has chaired several international conferences and workshops.

Andrew J. Fleming (S'02–M'03) was born in Dingwall, U.K., in 1977. He received the B.E.E. and Ph.D. degrees from The University of Newcastle, Callaghan, Australia, in 2000 and 2004, respectively.

He is currently an Australian Research Council Fellow stationed at the School of Electrical Engineering and Computer Science, The University of Newcastle. His research includes nanopositioning, high-speed scanning probe microscopy, microcantilever sensors, and sensorless control of sound and vibration. He is an Associate Editor of *Advances in Acoustics and Vibration*. He is the coauthor of two books, several patent applications, and more than 100 journal and conference papers.

Dr. Fleming was the recipient of the University of Newcastle Vice-Chancellor's Award for Researcher of the Year in 2007. Also in 2007, he was a corecipient of the IEEE Control Systems Society Outstanding Paper Award for research published in the IEEE TRANSACTIONS ON CONTROL SYSTEMS TECHNOLOGY.